This is a peer-reviewed, accepted author manuscript of the following conference paper: Pepper, B & Campos-Gaona, D 2024, Impedance estimation for transient stability enhancement of virtual synchronous machines. in 2024 IEEE 15th International Symposium on Power Electronics for Distributed Generation Systems (PEDG). IEEE, Piscataway, NJ.

Impedance Estimation for Transient Stability Enhancement of Virtual Synchronous Machines

Benjamin Pepper
Department of Electronic and Electrical Engineering
University of Strathclyde
Glasgow, UK
Email: benjamin.pepper@strath.ac.uk

David Campos-Gaona
Department of Electronic and Electrical Engineering
University of Strathclyde
Glasgow, UK
Email: d.campos-gaona@strath.ac.uk

***Abstract*—In this paper, a passive technique for estimating the impedance and voltage of a Thévenin grid is presented. The method can be applied when either the maximum active power or minimum reactive power operating point, with respect to the power angle, is crossed. This work addresses transient events, for which the former occurs. A key assumption is that the power response of the converter is sufficiently slow such that the steady-state equations for active and reactive power remain accurate as the power angle varies, which is valid for virtual synchronous machines. In conjunction with the equal-area criterion, the estimated parameters are used to appropriately adjust the reference active power to maintain synchronism with the grid. The methodology is validated in MATLAB/Simulink.**

I. Introduction

In order to mitigate the effects of climate change, the prevalence of renewable, converter-based resources is increasing in power networks. While this is paramount, it poses challenges such as lower system inertia and short circuit ratio. Over the last couple of decades, grid-forming control has been developed as an alternative to grid-following which may be more stable in weak and faulty grids [1], [2], [3]. A virtual synchronous machine (VSM) is a type of grid-forming algorithm which can emulate the inertia and damping of a synchronous generator [4], and it is adopted in this study.

The transient stability of a generation unit refers to its ability to maintain synchronism with the grid when subjected to large disturbances, such as a transmission line fault [5]. The existing methods for enhancing the transient stability of synchronous generators include changing the active and/or reactive power reference, which is also applicable to VSMs. However, it is difficult to quantify a suitable change in reference without prior knowledge of the grid impedance and voltage at the receiving end of the network [1].

In the context of converter control, there are two main techniques for estimating the impedance of the equivalent receiving-end Thévenin grid [6]: active and/or reactive power variation, and injecting an inter-harmonic disturbance at the point of common coupling (PCC). P/Q variation was originally proposed for grid-following converters [7], and an adaptation to grid-forming has been presented [8]. However, the grid frequency is assumed to be known and constant in this adaptation. It is unclear if this approach would be applicable if the frequency were variable, unless it can be accurately estimated at a high sampling rate in real time. The inter-harmonic injection method is based on introducing a voltage and current frequency which is not already present in the grid [9]. While this technique can be implemented without online knowledge of the grid frequency, it is more intrusive than P/Q variation, and it seems there is not yet a comprehensive and relevant framework in the grid codes.

The impedance estimation problem for a converter connected to an infinite bus can be framed as an under-determined system of two equations in four unknowns. The independent equations are for the active and reactive power. Meanwhile, the unknowns are the power angle; the resistance and reactance of the grid; and the voltage at the receiving end of the grid. This paper proposes a passive technique for estimating the grid parameters which consists of measuring the maximum active power or minimum reactive power, with respect to the power angle, which can be delivered to the grid. The former occurs during transient events, while the latter operating point is situated at lower power angles. From this, four equations in four unknowns are obtained, and the system can be solved for the grid impedance and voltage.

The remainder of this paper is structured as follows. In Section II-A, a method for estimating the unknowns of a Thévenin grid is described. This is followed by Section II-B, where a basic means of detecting a change of network impedance is presented. Section II-C describes an approach for detecting the maximum active power operating point from the timeseries of active and reactive power. In Section II-D, it is shown how the estimated parameters can be used with the equal-area criterion to update the reference active power. The methodology is validated for two case studies in MATLAB/Simulink in Section III, and the key findings are summarised in Section IV.

II. Methodology

A. Impedance and Voltage Estimation

The system under study in this paper is presented in Fig. 1. The outer loop for the active power, P, is based on the swing equation [4], and a reference for the PCC voltage magnitude is selected rather than the reactive power, Q. There are two inner loops in cascade which control the PCC voltage and the current through the converter filter [2]. The network is represented as

a parallel impedance connected to an infinite bus. By opening the switch S, the network impedance can be increased and a large disturbance can be induced. The converter operated as a VSM behaves like an ac voltage source, and the circuit can be approximated by that shown in Fig. 2.

As in [8], a key assumption is that the power response of the converter is sufficiently slow such that the steady-state equations for active and reactive power remain accurate during the transient process, which is the case for VSMs. As such, P and Q after the fault are given by

$$P = \frac{V_o}{R_1^2 + X_1^2}\left[V_o R_1 + V_g(X_1 \sin\delta - R_1 \cos\delta)\right], \quad (1)$$

$$Q = \frac{V_o}{R_1^2 + X_1^2}\left[V_o X_1 - V_g(R_1 \sin\delta + X_1 \cos\delta)\right], \quad (2)$$

where V_o is the converter output voltage; V_g, R_1, and X_1 are the voltage, resistance, and reactance of the grid respectively; and the power angle δ is the phase difference between V_o and V_g [10]. These can be rewritten as

$$P = \frac{V_o}{R_1^2 + X_1^2}\left[V_o R_1 + V_g\sqrt{R_1^2 + X_1^2}\sin(\delta - \phi)\right], \quad (3)$$

$$Q = \frac{V_o}{R_1^2 + X_1^2}\left[V_o X_1 - V_g\sqrt{R_1^2 + X_1^2}\cos(\delta - \phi)\right], \quad (4)$$

where $\phi = \arctan(R/X)$. By inspection, it can be seen that the maximum active power occurs at $\delta = \pi/2 + \phi$. Its value is given by

$$P_{\max} = \frac{V_o}{R_1^2 + X_1^2}\left(V_o R_1 + V_g\sqrt{R_1^2 + X_1^2}\right). \quad (5)$$

At this power angle, the reactive power is equal to its offset value

$$Q_0 = \frac{X_1 V_o^2}{R_1^2 + X_1^2}. \quad (6)$$

If the active and reactive power are measured at another power angle $\delta_i \neq \pi/2 + \phi$ (Fig. 3)

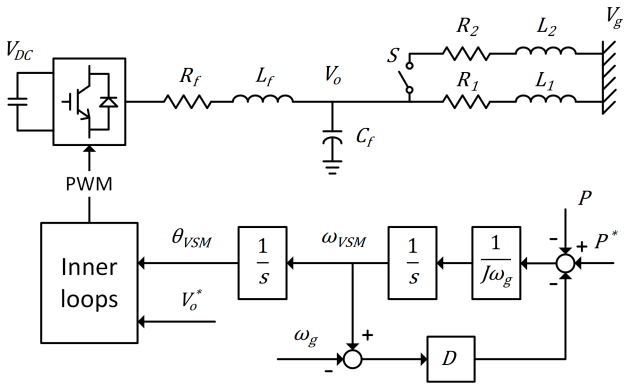

Fig. 1. Control structure of the VSM and the system under study.

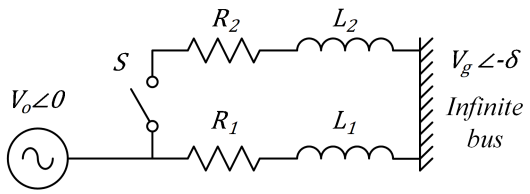

Fig. 2. An approximation to the system in Fig. 1.

$$P_i = \frac{V_o}{R_1^2 + X_1^2}\left[V_o R_1 + V_g\sqrt{R_1^2 + X_1^2}\sin(\delta_i - \phi)\right], \quad (7)$$

$$Q_i = \frac{V_o}{R_1^2 + X_1^2}\left[V_o X_1 - V_g\sqrt{R_1^2 + X_1^2}\cos(\delta_i - \phi)\right], \quad (8)$$

then (5)–(8) constitute a system of four equations in four unknowns, which can be solved simultaneously for the grid impedance and voltage. To this end, it is useful to rewrite (5)–(8) as

$$P_i = AV_o + C, \quad (9)$$

$$Q_i = BV_o - D, \quad (10)$$

$$P_{\max} = AV_o + \sqrt{C^2 + D^2}, \quad (11)$$

$$Q_0 = BV_o, \quad (12)$$

where [8]

$$A = \frac{V_o R_1}{R_1^2 + X_1^2}, \quad (13)$$

$$B = \frac{V_o X_1}{R_1^2 + X_1^2}, \quad (14)$$

$$C = V_g(B\sin\delta_i - A\cos\delta_i), \quad (15)$$

$$D = V_g(A\sin\delta_i + B\cos\delta_i). \quad (16)$$

Equations (9)–(10) can then be solved as

$$B = \frac{Q_0}{V_o}, \quad (17)$$

$$D = BV_o - Q_i, \quad (18)$$

$$C = \frac{D^2 - (P_{\max} - P_i)^2}{2(P_{\max} - P_i)}, \quad (19)$$

$$A = \frac{P_i - C}{V_o}. \quad (20)$$

Finally, the impedance and grid voltage magnitude are found by inverting (13)–(16):

$$R_1 = \frac{V_o A}{(A^2 + B^2)}, \quad (21)$$

$$X_1 = \frac{V_o B}{(A^2 + B^2)}, \quad (22)$$

$$V_g = \sqrt{\frac{C^2 + D^2}{A^2 + B^2}}. \quad (23)$$

Equations (21)–(23) are the estimated grid impedance and voltage for a single measurement pair of P_i and Q_i. If there were significant noise in the system, it may be beneficial to solve (5)–(8) for multiple measurement pairs, and compute an appropriate statistical average. In this paper, however, the methodology is tested via simulation, with no modelling of noise. Therefore, a detailed analysis of its effects is not presented here.

An alternative system of four equations could be made by considering the minimum value of reactive power, which occurs at $\delta = \phi$ (Fig. 3)

$$Q_{\min} = \frac{V_o}{R_1^2 + X_1^2}\left(V_o X_1 - V_g\sqrt{R_1^2 + X_1^2}\right). \tag{24}$$

The corresponding value of active power is

$$P_0 = \frac{R_1 V_o^2}{R_1^2 + X_1^2}. \tag{25}$$

Applying a similar approach to the above, (7), (8), (24), and (25) could be solved for the unknowns. However, since this study relates to transient stability when the power angle exceeds $\pi/2 + \phi$, the solution derived from (5)–(8) is used in the subsequent sections.

B. Fault Detection

In Fig. 2, the opening of switch S at $t = t_s$ is a simplified representation of circuit breakers opening following a fault. It is well-known that the fault current for RL circuits consists of a steady-state ac term and a dc offset which decays exponentially [10]. It is also known that while positive sequence signals correspond to constant direct and quadrature terms, dc terms are contained in the 0-sequence [11].

In the dq0 frame, the instantaneous power delivered to the grid is given by

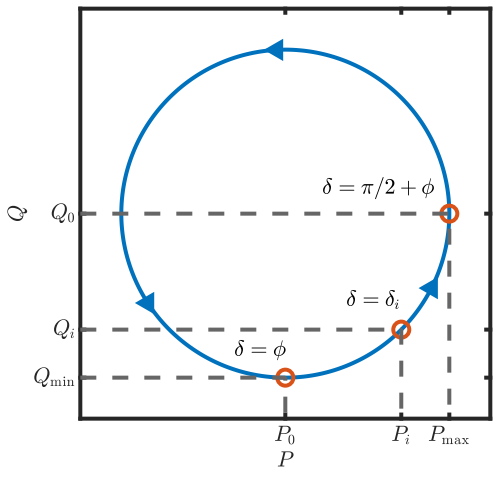

Fig. 3. A parametric curve of active and reactive power as a function of the power angle. The grid impedance and voltage can be estimated if (P_i, Q_i) and $(P_{\max}, Q_0)$ are measured. If the system operates at lower power angles, $(P_0, Q_{\min})$ could be used instead of $(P_{\max}, Q_0)$.

$$p = \frac{3}{2}(v_{\mathrm{d}} i_{\mathrm{d}} + v_{\mathrm{q}} i_{\mathrm{q}} + 2 v_0 i_0), \tag{26}$$

where v_{d}, v_{q}, and v_0 are the dq0 components of the PCC voltage; and i_{d}, i_{q}, and i_0 are those of the line current. Based on the above discussion, the transient power after the fault will be contained solely in the 0-sequence current and voltage. Meanwhile, the d and q terms represent the steady-state power. The event can be detected by considering the ratio of transient power to steady-state power

$$r = \frac{2 v_0 i_0}{v_{\mathrm{d}} i_{\mathrm{d}}}, \tag{27}$$

where the q term is ignored because the reference $v_{\mathrm{q}}^* = 0$. A threshold T can be chosen such that $|r| > T$ indicates that a fault may have occurred. After the fault, it is observed that the active power takes a short but finite time to drop to its post-fault value. Once the event is detected, a short delay is included to accommodate for this before collecting measurements of P and Q.

C. Maximum Active Power Transfer Detection

A key aspect of this approach is that $P_{\max}$ can be detected even though only the timeseries of P and Q are available. As highlighted by (3) and (4), the active power leads the reactive power by $\pi/2$ radians for all values of the grid impedance and voltage. This implies that the active power has reached its maximum value with respect to the power angle, $P_{\max}$, when the derivative $\mathrm{d}P/\mathrm{d}t$ becomes negative while $\mathrm{d}Q/\mathrm{d}t$ remains positive (Fig. 3). To reduce the effects of noise, filtered derivatives are considered in this study. The criteria can then be stated as

$$\frac{sP}{\tau s + 1} < 0, \tag{28}$$

$$\frac{sQ}{\tau s + 1} > 0, \tag{29}$$

where s is the Laplace variable, and the time constant τ represents the delay of the first-order low-pass filter. The time constant is selected to be as low as possible without noise interfering with the criteria above. Since there is a delay between detection of the maximum and when it occurs, buffers for the P and Q measurements are used. Once (28) and (29) are satisfied, the maximum value of P in the buffer is selected as $P_{\max}$. The index of $P_{\max}$ is then used to locate and select the corresponding value of Q, which is the offset Q_0.

D. Active Power Reference Adjustment

The active power reference is updated according to the equal-area criterion. In the pre-fault condition, consider a VSM in equilibrium with an initial power angle δ_0 (Fig. 4). After the fault, the reference power P_0^* is greater than the post-fault active power, and the VSM accelerates to increase its power angle. The area A_1 bounded by the reference P_0^* and the active power is known as the acceleration area. Once the maximum active power has been detected and measured at

δ_1, the estimated grid impedance and voltage can be used to update the reference power to P_1^*. The equal area criterion states that the power angle will increase until the deceleration area, A_2, equals the acceleration area [10]. The power angle at which this occurs is labelled δ_2. At δ_2, the VSM begins to swing back and the active power eventually settles at P_1^*.

Applying the equal area criterion, it can be shown that the updated reference is given by

$$P_1^*(\delta_2) = \frac{\int_{\delta_1}^{\delta_2} P \, \mathrm{d}\delta - A_1}{\delta_2 - \delta_1}. \tag{30}$$

The maximum power angle δ_2 is an independent parameter, and there is a range of options for constructing the deceleration area A_2. A lower reference P_1^* would correspond with a lower maximum power angle. However, it would also imply settling in a final state which exports less active power, and imposing a larger deceleration on the VSM which may be undesirable if it were supplied by a wind turbine, for example. The value of δ_2 which maximizes P_1^* can be found by solving $\partial P_1^*/\partial\delta_2 = 0$. This gives

$$P(\delta_2)(\delta_2 - \delta_1) = \int_{\delta_1}^{\delta_2} P \, \mathrm{d}\delta - A_1, \tag{31}$$

which can be worked through to

$$\sin(\delta_2 - \phi)(\delta_2 - \delta_1) + \cos(\delta_2 - \phi) = E, \tag{32}$$

where the constant E is given by

$$E = \cos(\delta_1 - \phi) - A_1 \frac{\sqrt{R_1^2 + X_1^2}}{V_o V_g}. \tag{33}$$

Equation (32) can be solved numerically for δ_2. Alternatively, if detection of the maximum is faster than the VSM dynamics then the approximation $\delta_1 \approx \pi/2 + \phi$ can be used. Equation (32) then becomes

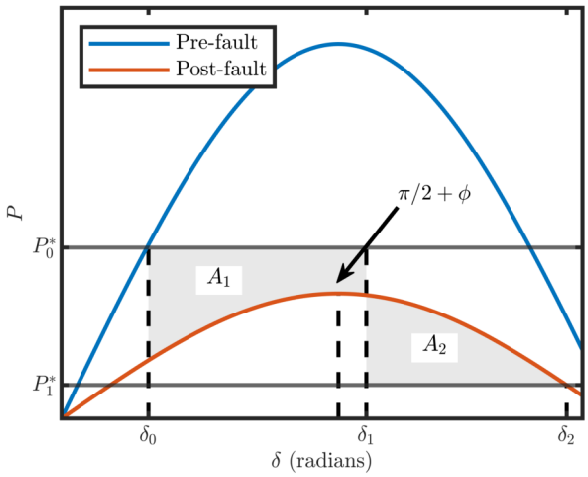

Fig. 4. The equal-area criterion for Type II transient stability, which is defined by $P_0^* > P_{\max}$ [5].

TABLE I
SIMULATION PARAMETERS

General			
Parameter	**Value**	**Parameter**	**Value**
$\boldsymbol{P_{\text{base}}}$	10 MW (1 p.u.)	$\boldsymbol{V_g}$	1 p.u.
$\boldsymbol{V_{\text{base}}}$	690 (1 p.u.)	$\boldsymbol{R_f}$	0.01 p.u.
$\boldsymbol{\omega_g}$	$2\pi \cdot 50$ rad/s (1 p.u.)	$\boldsymbol{L_f}$	0.1 p.u.
$\boldsymbol{P_0^*}$	1 p.u.	$\boldsymbol{C_f}$	0.1 p.u.
$\boldsymbol{V_o^*}$	1 p.u.	$\boldsymbol{t_s}$	0.5 s
$\boldsymbol{H}$ [a]	2 s	$\boldsymbol{T}$	1 %
$\boldsymbol{D}$	150 p.u.	$\boldsymbol{\tau}$	0.1 s

Case Study 1			
Parameter	**Value (p.u.)**	**Parameter**	**Value (p.u.)**
$\boldsymbol{R_1}$	0.15	$\boldsymbol{R_2}$	0.075
$\boldsymbol{L_1}$	1.5	$\boldsymbol{L_2}$	0.75

Case Study 2			
Parameter	**Value (p.u.)**	**Parameter**	**Value (p.u.)**
$\boldsymbol{R_1}$	1.27	$\boldsymbol{R_2}$	1.48
$\boldsymbol{L_1}$	1.27	$\boldsymbol{L_2}$	1.48

[a] The inertia constant H is defined by $H = \frac{1}{2} J \omega_g^2 / P_{\text{base}}$.

$$\left(x - \frac{\pi}{2}\right)\sin x + \cos x = -\frac{A_1\sqrt{R_1^2 + X_1^2}}{V_o V_g}, \tag{34}$$

where $x = \delta_2 - \phi$. The lowest order expansion of (34) around $x = \pi/2$ is

$$\frac{(x - \pi/2)^3}{3} = \frac{A_1\sqrt{R_1^2 + X_1^2}}{V_o V_g}, \tag{35}$$

which gives a maximum power angle of

$$\delta_2 = \delta_1 + \left(\frac{3A_1\sqrt{R_1^2 + X_1^2}}{V_o V_g}\right)^{1/3}. \tag{36}$$

The updated reference is then given by $P_1^* = P(\delta_2)$.

III. Results and Discussion

The methodology outlined in the previous section is tested in MATLAB/Simulink for two case studies. The ratio of grid resistance to reactance is $1:10$ for case study 1, and $1:1$ for case study 2. These ratios are typical of high- and medium-voltage lines, respectively [12]. The simulation parameters are presented in Table I. In the pre-fault state, the reference power is $P_0^* = 10$ MW. After the fault is detected, the first hundred measurements of P and Q are recorded, and the grid impedance and voltage is estimated for each measurement. The mean values of these estimates are then computed, and presented in Tables II and III.

TABLE II
CASE STUDY 1

	True Value	Estimation	Relative Error (%)
$\boldsymbol{R_1}$	0.150 p.u.	0.157 p.u.	4.67
$\boldsymbol{X_1}$	1.50 p.u.	1.51 p.u.	0.667
$\boldsymbol{V_g}$	1.00 p.u.	1.00 p.u.	0
$\boldsymbol{A_1}$	4.83 MW · rad	4.86 MW · rad	0.6
$\boldsymbol{A_2'}$	153 kW · rad	-	-

A. Case Study 1

The switch S opens at $t_s = 0.5$ s. As shown in Fig. 5, there is a sharp rise in the ratio of transient to steady-state power, and the event is detected at 0.502 s. Subsequently, the active power delivered to the network reaches its maximum value at 1.00 s, and it is detected at 1.11 s. The delay of approximately 100 ms is consistent with the time constant τ of the low-pass filter. In Table II, the estimated grid impedance and voltage are compared with their true values. It can be seen that the relative error for all estimates is less than 5%, which is comparable to other impedance estimation techniques [6].

Solving (32) numerically, the power angle which maximises the updated reference is found to be $\delta_2 = 183°$. This corresponds with a reference of $P_1^* = 1.00$ MW. However, the maximum power angle which is reached in the simulation is just 109°. This is illustrated in Fig. 6, where δ_2' and A_2' are the maximum power angle and deceleration area of the simulation, respectively. Given that A_2' is the deceleration area which was required in the simulation, solving (32) for $A_1 = A_2'$ indicates that P_1^* could have been as high as 6.37 MW without causing rotor-angle instability. This very large margin for error is attributed to the damping of the VSM, which is not taken into account by the equal-area criterion.

B. Case Study 2

A similar analysis can be applied for the second case study. The delays for detecting the fault and the active power maximum are 4 ms and 83 ms, respectively. To three significant figures, the relative error for the resistance and reactance are both zero (of course, it is expected that the error would be larger if there were noise). The lower relative error for this case may be because the power response is slower (Fig. 7), and therefore the implicit steady-state assumption of (1) and (2) is more accurate, and because the resistance is an order of magnitude larger. Interestingly, though, the relative error for A_1 is slightly less in case study one.

The updated reference is found to be $P_1^* = 6.34$ MW. However, Table III shows that $A_1/A_2' = 415$. Using the same approach as case study 1, the updated reference could have been as high as 9.46 MW without causing loss of synchronism with the grid. The conservative result of the equal-area criterion provides a margin against error in the estimated parameters, but it also implies settling in a final operating point which exports less active power. This could be addressed by updating the active power reference on more than one occasion. For example, once it is detected that the power angle has returned over $\pi/2 + \phi$, then the reference could be updated to any value less than $P_{\max}$.

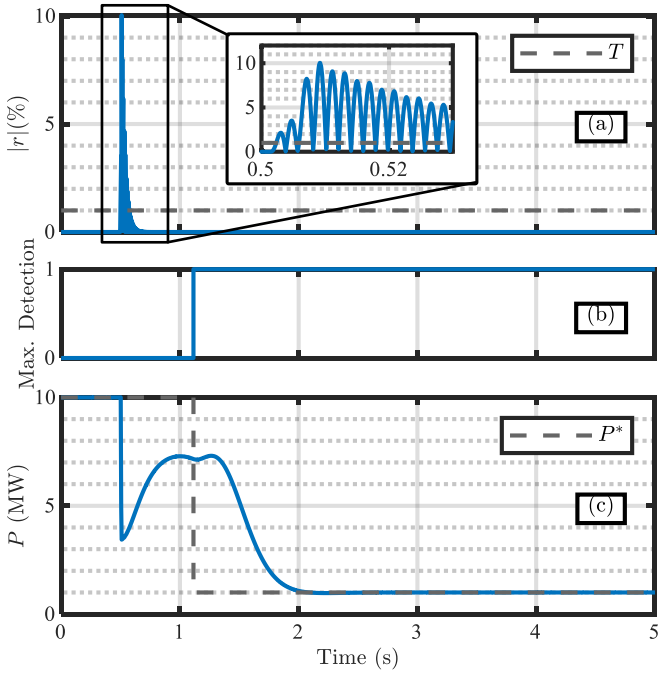

Fig. 5. (a) The ratio of transient to steady-state power, $|r|$, exceeds the threshold, T, after the fault. (b) The maximum active power is detected using (28)–(29). (c) The active power reference is updated so that the VSM maintains synchronism with the grid.

IV. CONCLUSION

In this paper, a passive method for estimating the impedance and voltage of a Thévenin grid has been presented. The method can be applied when the maximum active power or minimum

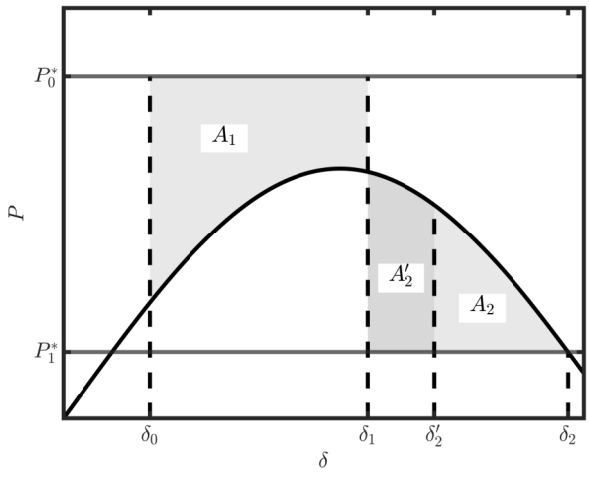

Fig. 6. According to the equal-area criterion, the deceleration area, A_2, equals the acceleration area, A_1. Due to the damping of the VSM, however, the deceleration area in the simulation, A_2', is much less than A_1.

TABLE III
CASE STUDY 2

	True Value	Estimation	Relative Error (%)
$\boldsymbol{R_1}$	1.27 p.u.	1.27 p.u.	0
$\boldsymbol{X_1}$	1.27 p.u.	1.27 p.u.	0
$\boldsymbol{V_g}$	1.00 p.u.	0.999 p.u.	0.1
$\boldsymbol{A_1}$	2.22 MW · rad	2.24 MW · rad	0.901
$\boldsymbol{A_2'}$	5.35 kW · rad	-	-

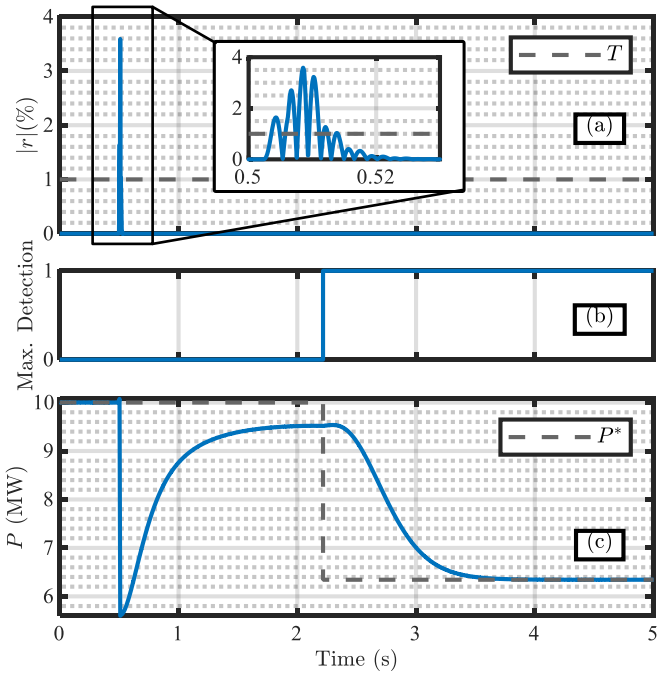

Fig. 7. (a) The fault is detected when the ratio of transient to steady-state power, $|r|$, exceeds the threshold, T. (b) The maximum active power is detected when (28)–(29) are satisfied. (c) Once the maximum has been detected, the active power reference is updated to maintain the rotor-angle stability of the VSM.

reactive power operating point, with respect to the power angle, is crossed. This study considers transient events, for which the former occurs. The advantages of this technique include that it is passive and it only requires local measurements at the PCC. On the other hand, it requires crossing one of either two specific operating points, as described above. It also relies on the power dynamics being slow enough such that the steady-state equations for active and reactive power remain accurate as the power angle varies. For the two case studies presented in the paper, the maximum relative error for any of the estimated parameters was 4.67%, and all others were below 1%. This is as accurate as or more accurate than previously proposed estimation techniques [6].

The estimated parameters are used in conjunction with the equal-area criterion to appropriately update the reference power in order to maintain synchronism with the grid. Since the equal-area criterion does not account for the VSM's damping, it gave a very conservative underestimate of the allowable reference power. While this provides some safety against error in the estimates, in future work the reference could be updated more than once. Other extensions to this work could include an investigation into the robustness of the technique against external disturbances such as measurement noise, and generalisation to multi-machine systems.

REFERENCES

[1] X. Wang, M. G. Taul, H. Wu, Y. Liao, F. Blaabjerg, and L. Harnefors, "Grid-synchronization stability of converter-based resources—an overview," *IEEE Open Journal of Industry Applications*, vol. 1, pp. 115–134, 2020.

[2] R. Rosso, X. Wang, M. Liserre, X. Lu, and S. Engelken, "Grid-forming converters: Control approaches, grid-synchronization, and future trends—a review," *IEEE Open Journal of Industry Applications*, vol. 2, pp. 93–109, 2021.

[3] J. Matevosyan, B. Badrzadeh, T. Prevost, E. Quitmann, D. Ramasubramanian, H. Urdal, S. Achilles, J. MacDowell, S. H. Huang, V. Vital *et al.*, "Grid-forming inverters: Are they the key for high renewable penetration?" *IEEE Power and Energy magazine*, vol. 17, no. 6, pp. 89–98, 2019.

[4] S. D'Arco and J. A. Suul, "Virtual synchronous machines—classification of implementations and analysis of equivalence to droop controllers for microgrids," in *2013 IEEE Grenoble Conference*. IEEE, 2013, pp. 1–7.

[5] P. Kundur, "Power system stability," *Power system stability and control*, vol. 10, pp. 7–1, 2007.

[6] M. K. De Meerendre, E. Prieto-Araujo, K. H. Ahmed, O. Gomis-Bellmunt, L. Xu, and A. Egea-Àlvarez, "Review of local network impedance estimation techniques," *IEEE access*, vol. 8, pp. 213 647–213 661, 2020.

[7] S. Cobreces, E. J. Bueno, D. Pizarro, F. J. Rodriguez, and F. Huerta, "Grid impedance monitoring system for distributed power generation electronic interfaces," *IEEE Transactions on Instrumentation and Measurement*, vol. 58, no. 9, pp. 3112–3121, 2009.

[8] J. Sun, J. Yu, J. Qiu, and Y. Wang, "Transient-responses-based grid impedance estimation for grid-forming converters," in *2022 4th International Conference on Electrical Engineering and Control Technologies (CEECT)*. IEEE, 2022, pp. 741–745.

[9] L. Asiminoaei, R. Teodorescu, F. Blaabjerg, and U. Borup, "Implementation and test of an online embedded grid impedance estimation technique for pv inverters," *IEEE Transactions on Industrial Electronics*, vol. 52, no. 4, pp. 1136–1144, 2005.

[10] J. D. Glover, M. S. Sarma, and T. Overbye, *Power system analysis & design, SI version*. Cengage Learning, 2012.

[11] C. J. O'Rourke, M. M. Qasim, M. R. Overlin, and J. L. Kirtley, "A geometric interpretation of reference frames and transformations: dq0, clarke, and park," *IEEE Transactions on Energy Conversion*, vol. 34, no. 4, pp. 2070–2083, 2019.

[12] J. Rocabert, A. Luna, F. Blaabjerg, and P. Rodriguez, "Control of power converters in ac microgrids," *IEEE transactions on power electronics*, vol. 27, no. 11, pp. 4734–4749, 2012.